NPL
National Physical Laboratory

NPL REPORT AC 24

STUDY OF THE IN-SITU CALIBRATION OF HYDROACOUSTIC SENSORS

PETER HARRIS, STEPHEN ROBINSON AND LIAN WANG

DECEMBER 2023

STUDY OF THE IN-SITU CALIBRATION OF HYDROACOUSTIC SENSORS

Peter Harris
Data Analytics and Modelling group

Stephen Robinson and Lian Wang
Ultrasound and Underwater Acoustics group

ISSN 1754-2936

https://doi.org/10.47120/npl.AC24

National Physical Laboratory
Hampton Road, Teddington, Middlesex, TW11 0LW

Approved on behalf of NPLML by
Louise Wright, Head of Science for the Data Science department.

CONTENTS

1 BACKGROUND

The Joint Research Project 19ENV03 “Infra-AUV” of the European Metrology Programme for Innovation and Research (EMPIR) [Infra-AUV] has delivered traceable calibration of acoustic, underwater, and seismic sensors for measurements at low frequencies, as well as improved knowledge of their performance in-situ. Various case studies have been used to demonstrate the impact for different end-user communities of that traceability and improved knowledge. As a component to achieving traceability from primary standards to a sensor deployed in the field, the project has investigated methods for the in-situ calibration of a sensor to deliver a calibration curve for the sensor accompanied by uncertainty information.

The objective of the study described in this report is to understand the extent to which a mixture of sources of sound can be used for the in-situ calibration of the hydroacoustic sensors within the International Monitoring System (IMS) operated by the Commission for the Comprehensive Nuclear-Test-Ban Treaty (CTBT) [CTBTO]. For this purpose, the approach taken for the in-situ calibration of infrasound sensors described in Gabrielson (2011), Charbit (2015), Green (2021) and Demeyer (2023) is followed, which is based on the application of “Gabrielson’s method”, and extensions to that method, using data recorded by two sensors that are essentially co-located. Simulated data is used to understand the extent to which that method can be applied in the context of hydroacoustic sensors. The advantage of using simulated data is that different aspects of the calibration set-up can be controlled, for example, the distance between the sensors, and how similar are the sensor calibration functions, etc. However, consideration is also given to applying the method to real data gathered by sensors deployed in NPL’s Wraysbury reservoir. A further objective is to implement the approach described in Demeyer (2023) to evaluate the uncertainty associated with the calibration of one sensor considering the other sensor as a reference sensor for which calibration information, comprising a frequency response with associated uncertainties, is available.

The report is organised as follows. In Section 2 we describe the data used the study, and in Section 3 the method of analysis is presented. Section 4 contains the results and discussion of those results. Conclusions are given in Section 5. Finally, Section 8 contains the results in graphical form.

2 DATA

Data for this study are generated in three ways. Firstly, using real data recorded by a hydroacoustic sensor within the IMS of the CTBT and information about the calibration of the sensors within that system. Secondly, using simulated data based on a simple model of how sound propagates in water. Finally, using real data recorded by calibrated hydroacoustic sensors deployed in NPL’s Wraysbury reservoir.

2.1 USING REAL DATA

The following three cases are considered:

A. The output signals for the hydroacoustic sensors are set equal to the data recorded over a four-day period by the hydrophone H01W1 located at the hydroacoustic station at Cape Leeuwin. The data is collected with a sampling frequency of 250 Hz, and it is scaled to represent sound pressure in units of pascals and mean-centred. The data is illustrated in Figure 1. This case represents the ideal situation when the hydroacoustic sensors are identical and co-located, and considers real data recorded by a hydrophone within the IMS of the CTBT.

B. The output signals for the hydroacoustic sensors are given by filtering the data recorded by the hydrophone H01W1 (above) using, respectively, the (different) frequency responses for the hydrophones H11N1 and H11N2 located at the hydroacoustic station to the north of Wake Island. Since only the amplitude responses are available, it is assumed that the hydrophones H11N1 and H11N2 have the same, flat phase response. The amplitude responses are illustrated in Figure 2, and no uncertainty information is provided about those responses. Consequently, the frequency responses are treated as exactly known, although some of the structure in the amplitude responses evident in the figure (particularly for higher frequencies) is probably not real but a consequence of imperfections in their calibrations that would otherwise be explained by the uncertainties associated with responses. This case represents the situation when the hydroacoustic sensors are different and are co-located.

C. The effect of separating the hydrophones by a distance of 1 m is simulated by modifying the phase content of the signal recorded by one of the hydrophones to represent the additional distance travelled by the incoming sound to reach that hydroacoustic sensor compared to the other sensor. The assumption made here is that the sound travels as a plane wave along the line connecting the two hydrophones. This case represents a more realistic situation when the hydroacoustic sensors are different and not co-located but is made simple by assuming the sound originates from a single, distant source.

2.2 USING A SIMPLE MODEL OF NOISE PROPAGATION

A sound field is simulated in a way that is deterministic, in the sense that the sound field is known at any location, but it appears random to the hydroacoustic sensors, arising as the superposition of sound from many different sources. The sound field is required to have the property that the coherence between the field at two locations decreases with increasing distance between the locations. Specifically, the simulation involves the following assumptions and steps:

1. There are n_s sources of sound distributed randomly within the rectangular region $[-S, S] \times [-S, S]$ on the sea surface, i.e., at zero depth.

2. There are $n_r = 2$ hydroacoustic sensors located at $[0,0]$ and $[R, 0]$, respectively, and at a depth H.

3. The sound field at any location is represented as a signal (or time series) lasting for m_t time intervals each of length T. The complete signal representing the sensor input is created by concatenating signals that are simulated over each such time interval. The complete signal representing the sensor output, which accounts for the frequency response of the sensor, is also created by concatenating signals over each time interval where each of those signals is obtained by applying the frequency response of the sensor to the input signal simulated over the corresponding time interval. For a sampling frequency f_s, the signals are defined by timestamps:

$$t_{i,j} = (j-1)T + (i-1)\frac{1}{f_s}, \qquad i = 1, \dots, Tf_s, \qquad j = 1, \dots, m_t,$$

and, within each time interval, by frequencies

$$f_k = k\frac{1}{T}, \qquad k = 0, \ldots, \frac{Tf_s}{2}.$$

4. The information about the sound generated by a single source is defined in the frequency domain by a set of randomly assigned initial amplitude values $A_{k,0}$ and randomly assigned initial phase values $\phi_{k,0}$ corresponding to frequencies $f_k, k = 0, \ldots, Tf_s/2$. Once assigned the amplitudes are fixed (although in a more general treatment the amplitudes would vary with time). However, although the phase values are considered fixed within each time interval of length T, they change from time interval to time interval according to

$$\phi_{k,j,0} = \phi_{k,0} + 2\pi f_k (j-1)T,$$

where j is the index of the time interval.

5. A simple model is used to propagate the sound generated at a single source to the sound received by a sensor. The amplitude values are adjusted according to a model of simple spherical spreading, viz.,

$$A_k = \frac{A_{k,0}}{r},$$

where r is the distance between the source and the sensor. The phase values are adjusted considering the speed of sound c in water, viz.,

$$\phi_{k,j} = \phi_{k,j,0} + \frac{2\pi r f_k}{c}.$$

6. The input signal $x(t)$ in the jth time interval, represented by the values $x(t_{i,j})$ at times $t_{i,j}, i = 1, \ldots, Tf_s$, received by a sensor from a single source is evaluated as the inverse discrete Fourier transform applied to the frequency domain representation of the input signal defined by the amplitude and phase values for the source calculated in step 0. The complete signal for the jth time interval is then constructed as the superposition of the signals received from all sources.

7. The output signal $y(t)$ in the jth time interval, represented by the values $y(t_{i,j})$ at times $t_{i,j}, i = 1, \ldots, Tf_s$, recorded by a sensor from a single source is evaluated by filtering, in the frequency domain, the input signal using the amplitude and phase responses of the sensor, followed by applying the inverse Fourier transform to the resulting frequency domain representation of the output signal. The complete signal for the jth time interval is then constructed as the superposition of the signals recorded by the sensor for all sources.

8. Steps 4 to 7 are repeated for each time interval, $j = 1, \ldots, m_t$, and each source is allowed to move by a random distance and in a random direction from time interval to time interval, i.e., as a random walk across the sea surface. In this way, perturbations in the sound field are generated at each sensor location from time interval to time interval. Specifically, a perturbation $(\delta_1, \delta_2)s$ is applied to the coordinates defining the location of each single source, with δ_1 and δ_2 independent random draws from the uniform distribution on $[-1, +1]$ (defining the direction of motion) and s a random draw from the uniform distribution on $[0, \Delta_s]$ (defining the distance moved). Here, Δ_s

controls how far the sources move from time interval to time interval (equivalently, how fast they are moving). The complete signals (both sensor input and sensor output) across all time intervals are constructed by concatenating the corresponding signals for each time interval.

9. Steps 4 to 8 are repeated for both sensors, with the characteristics of the sources (their initial amplitude and phase values as well as their motion from time interval to time interval) replicated exactly.

For illustration, consider an example with

$$n_s = 100, S = 10\ \text{km}, R = 10\ \text{m}, H = 2\ \text{km}, m_t = 60, T = 60\ \text{s}, f_s = 250\ \text{Hz}, \Delta_s = 100\ \text{m}.$$

Figure 3 shows snapshots of the input signals constructed in this way for two hydroacoustic sensors (identified as A and B) over intervals of lengths $m_t T = 3600$ s, $T = 60$ s, and 1 s. Figure 2 shows the amplitude responses for the two sensors, considered to be H11N1 and H11N2, the first and second hydrophones at the hydroacoustic station north of Wake Island. The sensors have amplitude responses that are close but not identical and, in the absence of knowledge about the phase responses, the phase responses are assumed to be flat and identically zero. As before, in the absence of uncertainty information about the frequency responses for the sensors, those frequency responses are treated as exactly known. Figure 4 shows snapshots of the output signals for the two sensors for the same intervals used in Figure 3.

2.3 USING DATA RECORDED AT NPL'S WRAYSBURY RESERVOIR

Three hydrophones (see Table 1) were deployed at NPL's Wraysbury reservoir at a depth of 3 m. Two similar hydrophones (on channels 1 and 2) were essentially co-located and a third, different hydrophone (channel 3) was located at a distance of approximately 1.1 m from the co-located hydrophones. Signals were collected at a sampling frequency of 2.5 kHz, and then down sampled to a sampling frequency of 250 Hz to accord with the sampling frequency used at the hydroacoustic stations within of the IMS of the CTBT. Figure 5 shows a schematic of the deployment of the hydrophones at the reservoir, and Figure 6 shows the recorded data that lasts approximately 18 hours. The figure shows that the signals recorded on channels 1 and 2 are quite similar, except for the occasional presence of a 'spike' in the signal, whereas the signal recorded on channel 3 is quite different, albeit the hydrophones are only separated by 1.1 m. For this case, uncertainty information is provided about the amplitude responses for the hydrophones and so, unlike the previous cases, the amplitude responses are not treated as exact.

Table 1 Hydrophones deployed at NPL's Wraysbury reservoir.

Channel	Hydrophone	Serial
1	TC4033	#056
2	TC4033	#077
3	TC4040	#023

3 METHOD

The method of Gabrielson [Gabrielson (2011)] comprises the following steps.

The first step is to evaluate the *magnitude-squared coherence function* between the output signals recorded by the two sensors (identified as A and B). It is a function of frequency and measures on a scale from zero to one frequency-domain correlation between the two signals. It is defined by

$$C_{AB}(f) = \frac{|P_{AB}(f)|^2}{P_{AA}(f)P_{BB}(f)}$$

in terms of the power spectral densities $P_{AA}(f)$ and $P_{BB}(f)$ and the cross power spectral density $P_{AB}(f)$ of the two signals. The (cross) power spectral densities are evaluated over overlapping time windows of length λ_w with a Hann windowing function applied to each time window, and then averaged over the windows.

The second step is to evaluate the *relative amplitude and phase responses* for the two sensors as the frequency-dependent complex-valued gain $H_{BA}(f)$. The frequency response for sensor B relative to that for sensor A is given by

$$H_{BA}(f) = \frac{P_{BB}(f)}{P_{BA}(f)}$$

in terms of the power spectral density $P_{BB}(f)$ and the cross power spectral density $P_{BA}(f)$ of the two signals. The calculated gain $H_{BA}(f)$ for frequency f is only considered reliable in the case that the magnitude-squared coherence at frequency f is sufficiently close to unity.
The final step is to evaluate the *complex-valued frequency response* for sensor B given by

$$H_B(f) = H_{BA}(f)H_A(f),$$

where $H_A(f)$ is the complex-valued frequency response for sensor A, which is assumed to be known from a prior calibration of the sensor that takes the role of a reference sensor. Equivalently,

$$|H_B(f)| = |H_{BA}(f)||H_A(f)|$$

and

$$\text{ang}\,[H_B(f)] = \text{ang}\,[H_{BA}(f)] + \text{ang}\,[H_A(f)],$$

where $|z|$ and $\text{ang}\,[\text{z}]$ denote the magnitude and phase, respectively, of complex-valued z.

Extensions of the method are applied, and described below, based on those described in Charbit (2015), Green (2021) and Demeyer (2023). These extensions involve dividing the frequency interval into a number of frequency bands, dividing the sensor signals into a number of time segments, and applying Gabrielson's method to the filtered sensor data for each frequency band and time segment combination. For the frequencies within a frequency band, estimates of the magnitude and phase of the complex-valued gain are obtained by averaging the values of the magnitude and phase calculated for those time segments for which the magnitude-squared coherence function is sufficiently close to unity. The standard deviation and covariance of those values can be used to quantify the uncertainty associated with the estimates. The idea behind the approach is that different lengths of time segment and time window can be chosen for the different frequency bands. Additionally, a step of outlier rejection is applied before the calculations of the averages, standard deviations and covariances.

Specifically, let λ_d denote the length of the sensor signals, B the number of frequency bands defined by corner frequencies $[f_{l,0}, f_{l,1}]$, $\lambda_{l,s}, l = 1, \dots, B$, the segment length for the lth frequency band, and $\lambda_{l,w}, l = 1, \dots, B$, the window length for the lth frequency band. The following steps are applied for each frequency band $l = 1, \dots, B$:

1. Divide the signals into $J_l = \lfloor \lambda_d / \lambda_{l,s} \rfloor$ segments of length $\lambda_{l,s}$.
2. For each time segment $j = 1, \ldots, J_l$:
    a. Apply a bandpass filter (such as a Butterworth filter of a specified order) defined by corner frequencies $[f_{l,0}, f_{l,1}]$.
    b. Apply the Welch periodogram to evaluate the power spectral and cross power spectral densities using a Hann windowing function applied to time windows of length $\lambda_{l,w}$ with 50 % overlap.
    c. Evaluate the mean-squared coherence function and the complex-valued gain in terms of values of the power spectral and cross power spectral densities.
3. For each frequency f in the lth frequency band, identify the indices I_l of those time segments for which the values of the mean-squared coherence exceed a threshold γ $(0 < \gamma < 1)$.
4. For frequencies f within the lth frequency band, use the trimmed averages of the values of the magnitude and phase of the complex-valued gain for those time segments identified by indices I_l as estimates of, respectively, $|H_{BA}(f)|$ and $\mathrm{ang}[H_{BA}(f)]$. Furthermore, use the trimmed standard deviations of those values as the standard uncertainties for those estimates, and the sample covariance of the values as the covariance between the estimates.

In Green (2021) particular choices for the frequency bands (defined by their corner frequencies) and corresponding segment lengths $\lambda_{l,s}$ and window lengths $\lambda_{l,w}$ are proposed, but these relate to the case of calibrating infrasound measuring systems. For the results presented here that relate to the case of calibrating underwater acoustic measuring systems, we make the choices given in Table 2 [Schwardt (2023)].

Furthermore, the lengths $\lambda_{l,w}$ of the time windows are set to divide the time segments into eight overlapping windows with 50 % overlap. (This is the default choice made by MATLAB's "cpsd" function that uses Welch's averaged, modified periodogram method of spectral estimation.) A threshold $\gamma = 0.98$ is used to decide that a value of the magnitude-squared coherence function is sufficiently close to unity to be used in the estimation of the complex-valued gain. (This is the value proposed in Charbit (2015).) For the purposes of calculating trimmed statistics, outliers are defined as values more than 1.5 interquartile ranges above the upper quartile (75 percent) or below the lower quartile (25 percent). The method is useful when the data are not normally distributed.

Table 2 Parameter choices for the application of Gabrielson' method with extensions

Frequency band l	Corner frequencies $[f_{l,0}, f_{l,1}]$/Hz		Order n_l of Butterworth filter	Length $\lambda_{l,s}$ of time segment/s
1	0.05	0.15	2	700
2	0.14	0.35	2	250
3	0.32	0.70	2	150
4	0.60	1.50	3	30
5	1.50	50.0	4	20

Some experimentation may be needed to optimise the choice of parameters. It should be noted that the calculated standard uncertainty captures uncertainty contributions arising from variability in the recorded signals in the sense of a Type A evaluation of uncertainty [BIPM et

al (2008)] but not those arising from the choice of the parameters λ_d, $\lambda_{l,s}$ or $\lambda_{l,w}$ or other sources.

4 EXPERIMENTS, RESULTS, AND DISCUSSION

4.1 USING REAL DATA

Figure 7 shows results for Case A considering identical hydrophones that are co-located. This is the ideal case, and the results are 'perfect' in the sense that the proportion of time segments that are coherent is 100 % for every frequency and the estimate of the magnitude of the gain is one with no uncertainty.

Figure 8 shows results for Case B considering different hydrophones that are co-located. The proportion of time segments that are coherent is generally close to 100 %, and the estimates of the magnitudes of the gain are generally good, picking out the features of the measured gains with small uncertainties.

Figure 9 and Figure 10 show results for Case C considering different hydrophones that are separated by, respectively, 1 m and 10 m. The results are still acceptable, although the uncertainties associated with the estimates increases as the distance between the hydrophones increases and the coherence between the output signals decreases.

4.2 USING A SIMPLE MODEL OF NOISE PROPAGATION

The data is simulated using the following settings:

$$n_s = 100, S = 10\ \mathrm{km}, H = 2\ \mathrm{km}, m_t = 100, T = 500\ \mathrm{s}, f_s = 250\ \mathrm{Hz}, \Delta_s = 0\ \mathrm{m},$$

i.e., it is assumed there are 100 stationary sources of sound at the surface randomly located in a region of size $20\ \mathrm{km} \times 20\ \mathrm{km}$, the hydrophones are at a depth of $2\ \mathrm{km}$ at, or near to, the centre of the region, and the output signals last for $100 \times 500\ \mathrm{s}$ (approximately 14 hours) and are sampled at a frequency of $250\ \mathrm{Hz}$. Figure 11 and Figure 12 show results considering different hydrophones that are, respectively, co-located ($R = 0\ \mathrm{m}$) and separated by 1 m ($R = 1\ \mathrm{m}$).

For hydrophones that are co-located the results are generally good, again picking out the features of the measured gains with small uncertainties. However, even for a separation of 1 m, the degradation in the results is appreciable. The proportion of time segments that are coherent drops dramatically, particularly for the higher frequencies, and for some frequencies it is close to 0 %. The estimates of the gain have large uncertainties, and do not provide useful information about the relative frequency responses of the hydrophones.

4.3 USING DATA RECORDED AT NPL'S WRAYSBURY RESERVOIR

Figure 13, Figure 14 and Figure 15 show results for the two pairs of hydrophones defined by, respectively, channels 1 and 2 (similar hydrophones separated by $R = 0\ \mathrm{m}$) and channels 1 and 3 (different hydrophones separated by $R = 1.1\ \mathrm{m}$). The proportions of time segments that are coherent is generally very low for both pairs (Figure 13), only approaching 50 % for very low frequencies below the frequencies for which calibration information about the hydrophones is available.

For the first pair (Figure 14), the measured gains are close to one, because the hydrophones are similar, and the uncertainties associated with the measured values are evaluated in terms of the uncertainties for the individual amplitude responses using the method of BIPM et al (2008). Estimates of the gain are generally only available at frequencies below those at

which calibration information is provided, and those estimates are consistent with the hypothesis that the gains are approximately one for all frequencies, except around 1 Hz. A few, isolated estimates are also obtained in the interval between, approximately, 8 Hz and 10 Hz, and those estimates are inconsistent with the measured values in the interval.

For the second pair (Figure 15), the measured gains are different from one, because the hydrophones are different. Estimates of the gain are only available at frequencies below those at which calibration information is provided, and those estimates are consistent with the values based on the calibration information at higher frequencies.

For both pairs, the uncertainties associated with the estimates of the gain are quite large, except at isolated frequencies where there is only one time segment for which the outputs signals are coherent and, consequently, the standard deviation of the estimates for individual time segments is zero.

5 CONCLUSIONS

The results obtained using simulated data (whether based on real data provided by hydrophones located at the hydroacoustic stations in the IMS of the CTBT or simulated from scratch using a simple model for noise propagation) suggest that the method of “Gabrielson” with some extensions can be used to provide calibrations of hydrophones in situ provided that the hydrophones are close enough. However, the results obtained using real data recorded by hydrophones in a shallow reservoir suggest that there remain some challenges associated with applying the method, particularly around having hydrophones that are close enough to be considered as co-located and achieving coherent signals at the frequencies of interest. Additionally, there are clearly practical challenges around co-locating a reference hydrophone with an uncalibrated hydrophone when that uncalibrated hydrophone is in the deep ocean. Nevertheless, the results indicate that there is some hope that the method can be used to extend the calibrations of hydrophones to low frequencies at which calibration information is not normally available.

6 ACKNOWLEDGEMENTS

This work has been undertaken within the Joint Research project 19ENV03 “Infra-AUV” of the European Metrology Programme for Innovation and Research (EMPIR). The EMPIR is jointly funded by the EMPIR participating countries within EURAMET and the European Union. The views expressed in the paper are those of the authors and do not necessarily represent those of the CTBTO.

7 REFERENCES

BIPM, IEC, IFCC, ILAC, ISO, IUPAC, IUPAP, and OIML. Guide to the Expression of Uncertainty in Measurement, JCGM 100:2008. BIPM, 2008.

Demeyer, S., Kristoffersen, S. K., Le Pichon, A., Larsonnier, F., and Fischer, N. Contribution to Uncertainty Propagation Associated with On-Site Calibration of Infrasound Monitoring Systems. *Remote Sens.*, **15**, 1892, 2023. https://doi.org/10.3390/rs15071892

Charbit, M., Doury, B., and Marty, J. Evaluation of infrasound in-situ calibration method on a 3-month measurement campaign, in *2015 Infrasound Technology Workshop of the Provisional Technical Secretariat of the Comprehensive Nuclear-Test-Ban Treaty Organisation*, Vienna International Centre, Vienna, 2015.

CTBTO. Available online: www.ctbto.org

Gabrielson, T.B. In situ calibration of atmospheric-infrasound sensors including the effects of wind-noise-reduction pipe systems. *J. Acoust. Soc. Am.*, **130**, 1154–1163, 2011.

Green, D.N., Nippress, A., Bowers, D., and Selby, N.D. Identifying suitable time periods for infrasound measurement system response estimation using across-array coherence. *Geophys. J. Int.*, **226**, 1159–1173, 2021.

Infra-AUV. Joint Research Project 19ENV03 “Infra-AUV” Metrology for low-frequency sound and vibration https://www.ptb.de/empir2020/infra-auv/home/

Schwardt, M. Spreadsheet containing information about the filterbanks used within the CalxPy software for hydrophones (‘Hydro_Filterbank_CalxPy.ods’), private communication, 18th April 2023.

8 FIGURES

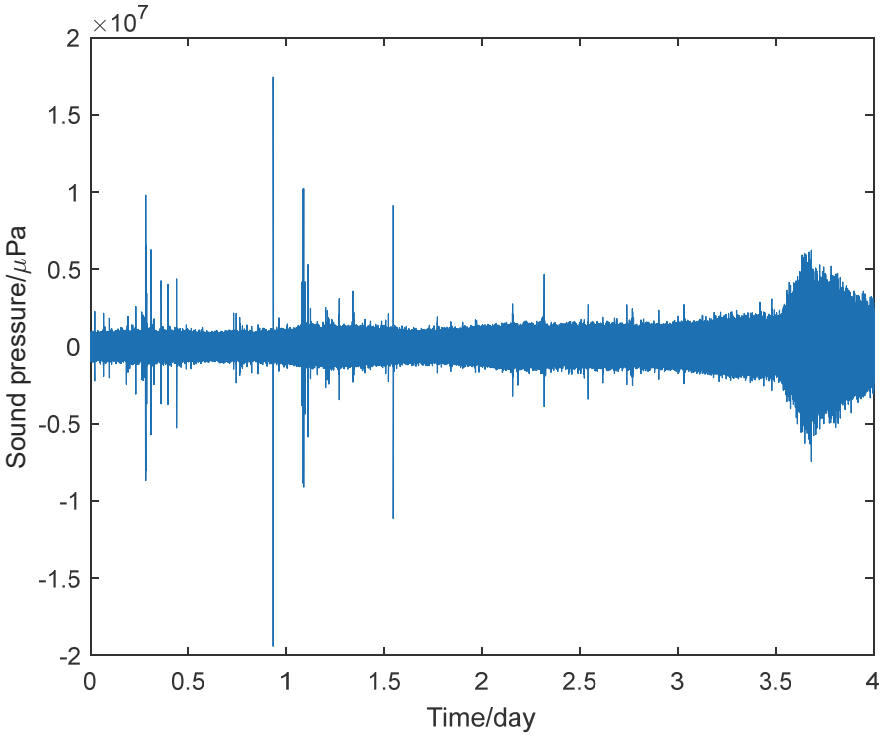

Figure 1 Sound pressure data collected by hydrophone H01W1 at the hydroacoustic station at Cape Leeuwin.

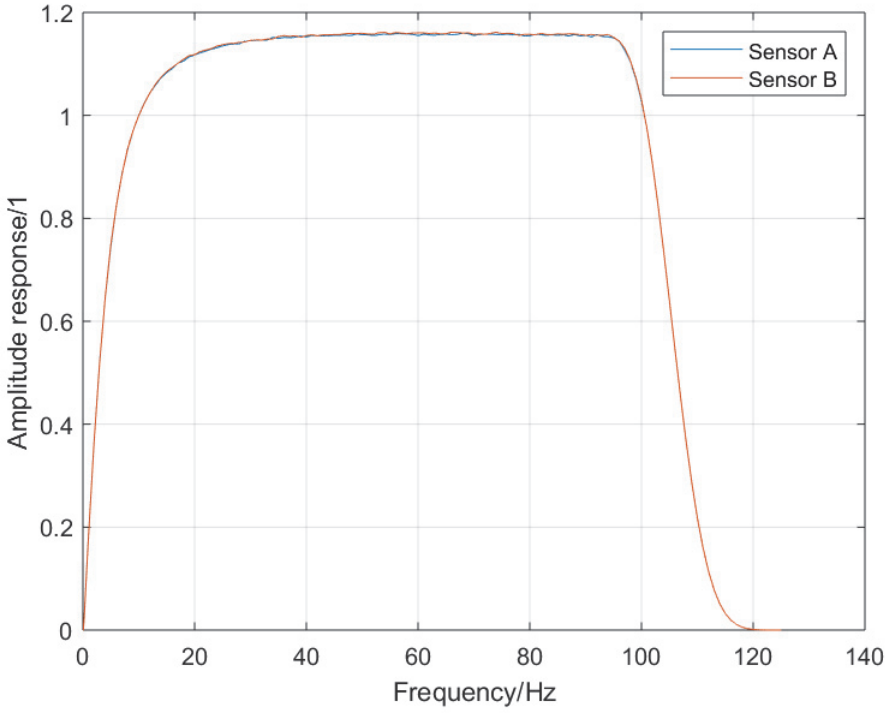

Figure 2 Frequency (amplitude) responses for the two hydrophones H11N1 (sensor A) and H11N2 (sensor B) at the hydroacoustic station to the north of Wake Island.

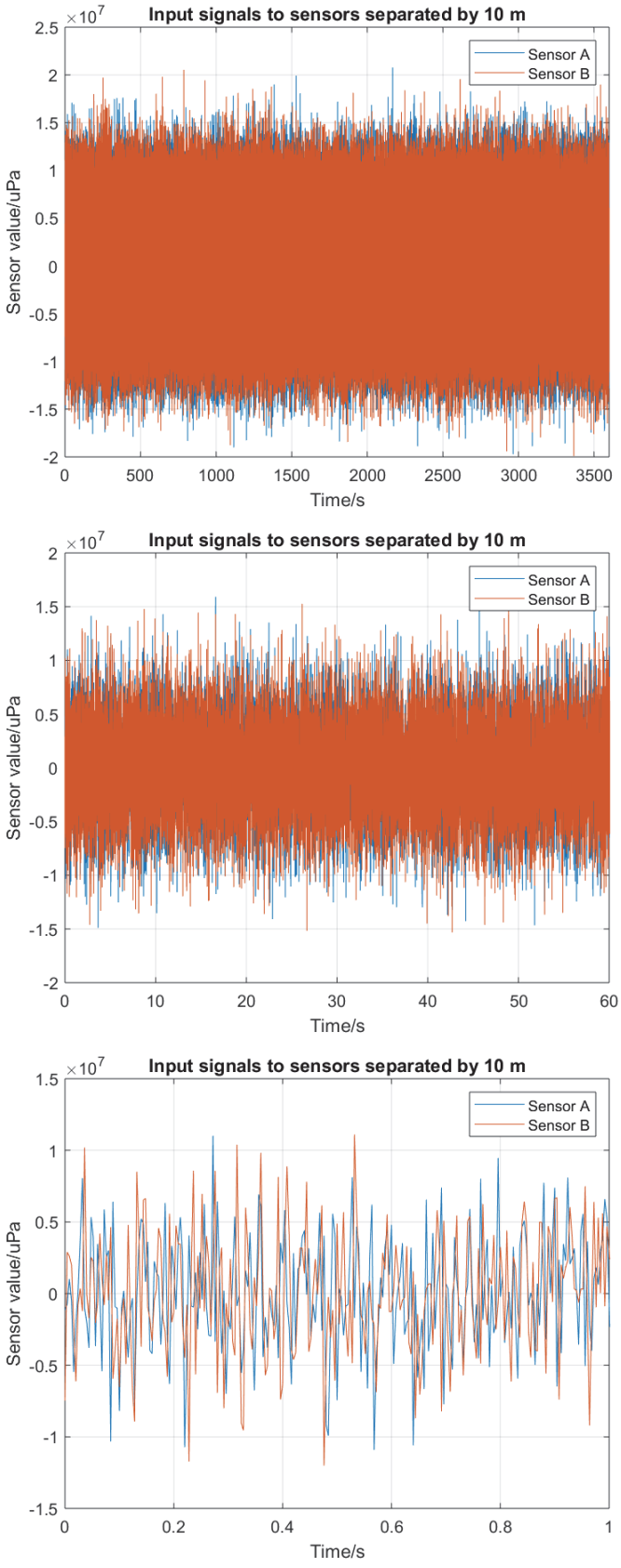

Figure 3 Snapshots of the input signals simulated for two sensors (H11N1 and H11N2) over intervals of $m_t T = 3600\ s$, $T = 60\ s$, and $1\ s$.

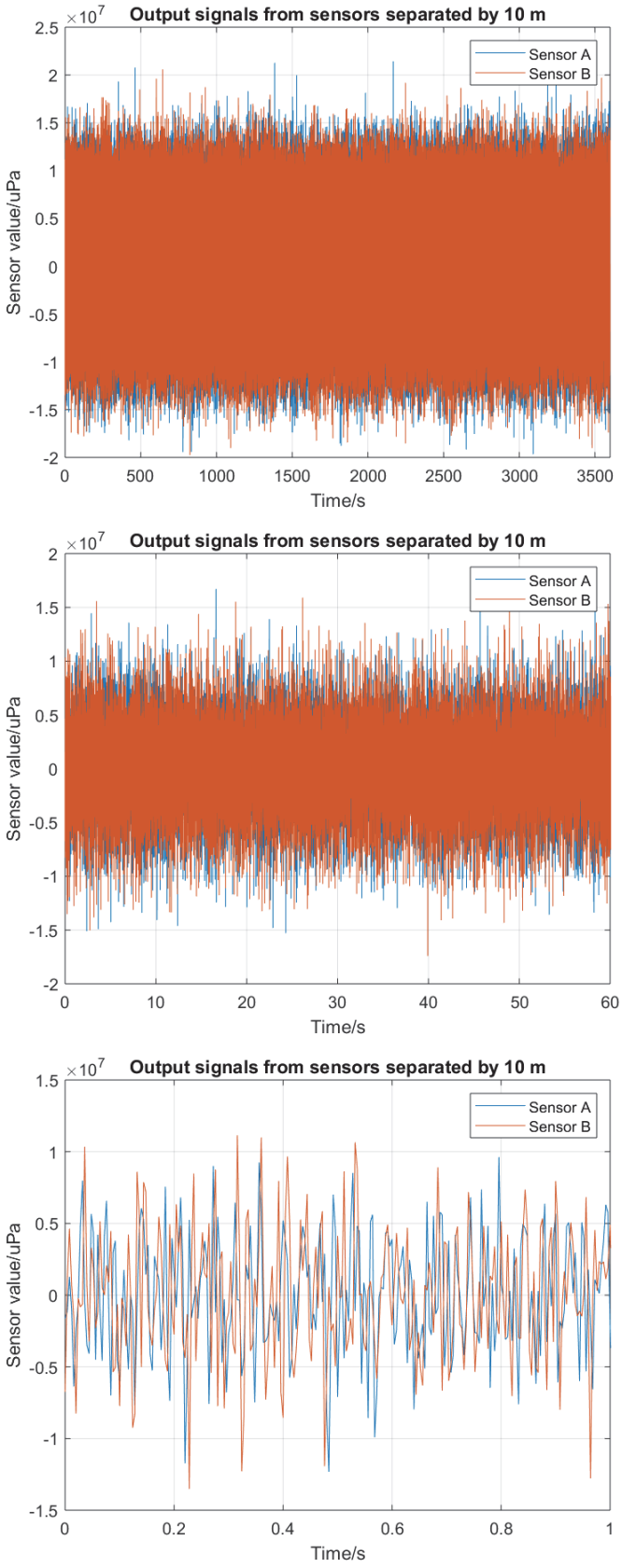

Figure 4 Snapshots of the output signals simulated for two sensors (H11N1 and H11N2) over intervals of $m_t T = 3600\ s$, $T = 60\ s$, and $1\ s$.

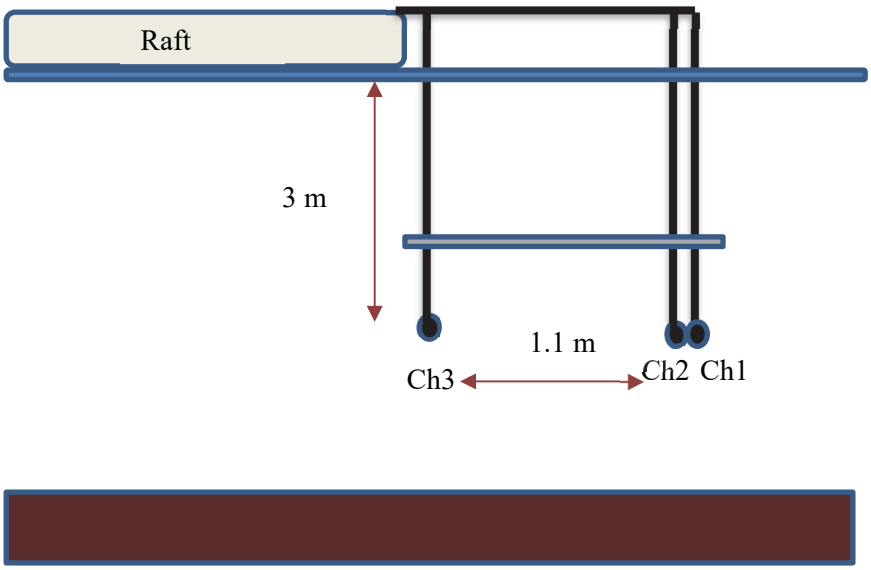

Figure 5 Schematic of deployment of hydrophones at NPL's Wraysbury reservoir.

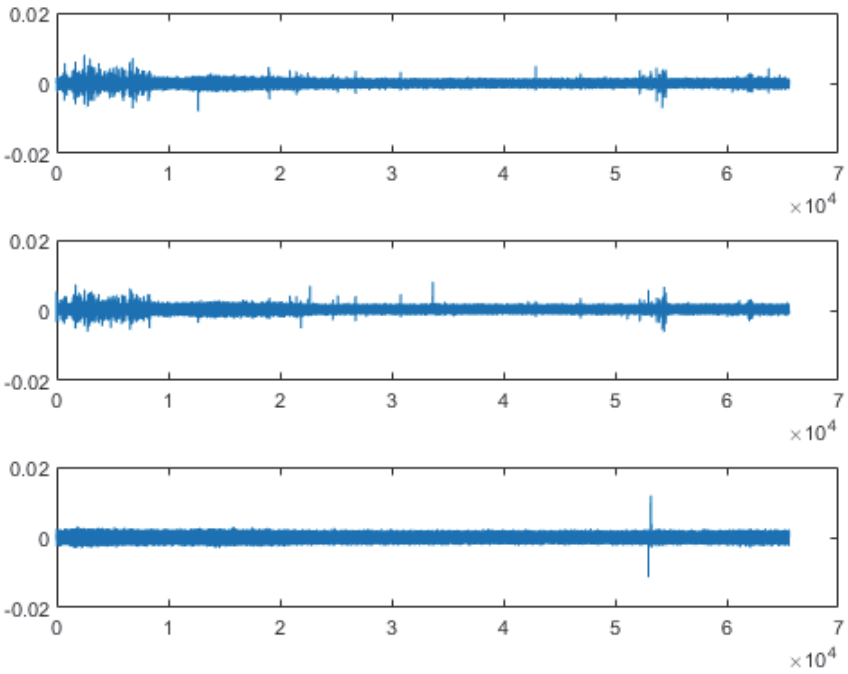

Figure 6 Data recorded by hydrophones deployed at NPL's Wraysbury reservoir: channel 1 (top), channel 2 (middle) and channel 3 (bottom). The horizontal axis is time in seconds.

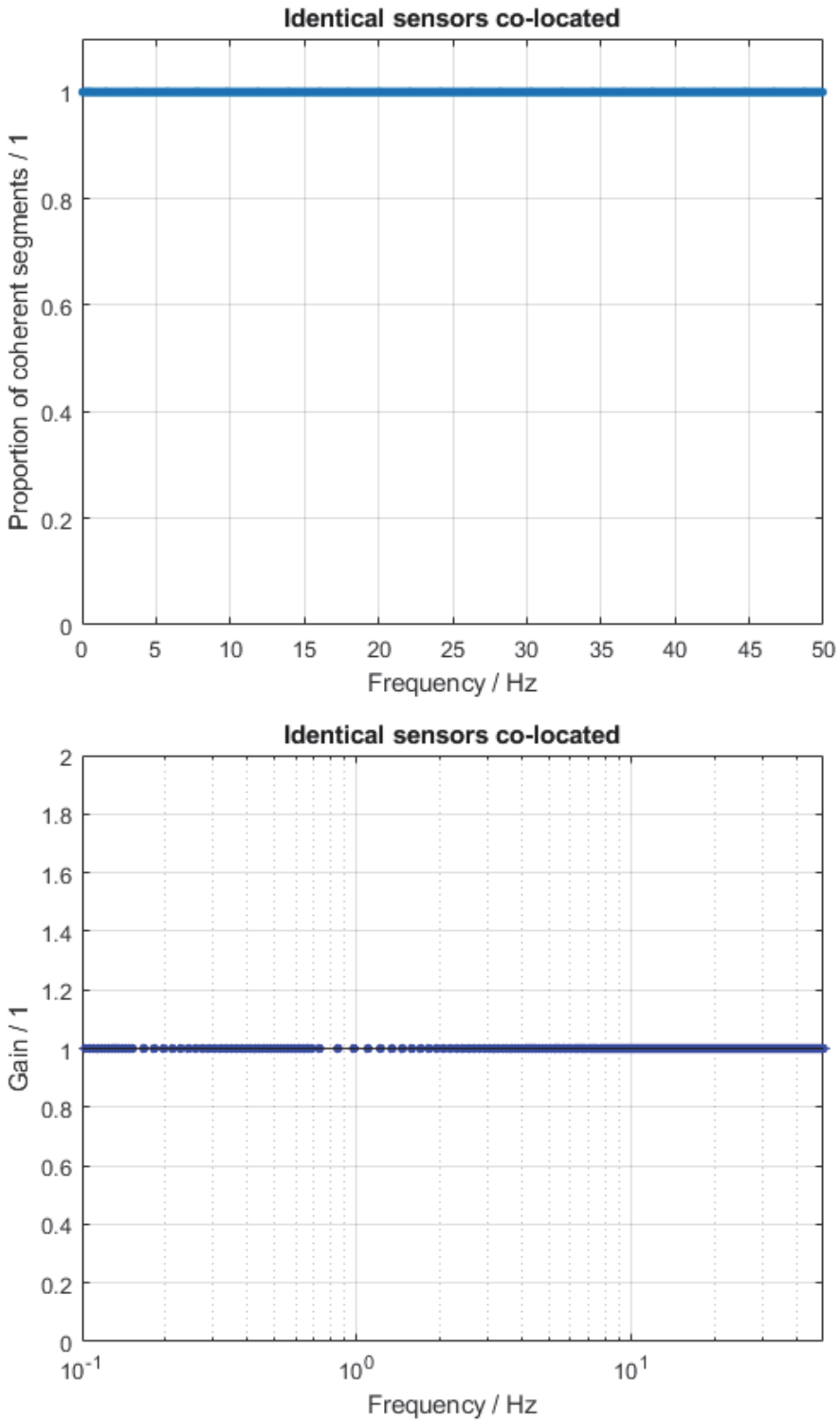

Figure 7 Results obtained using CTBTO data and Case A (identical sensors that are co-located). The top graph shows the proportion of time segments for which the magnitude-squared coherence function exceeds the threshold of 0.98. The bottom graph compares the known magnitude of the gain (which is equal to one for all frequencies) with the estimates (shown as blue dots). In this case, the estimates have zero uncertainty.

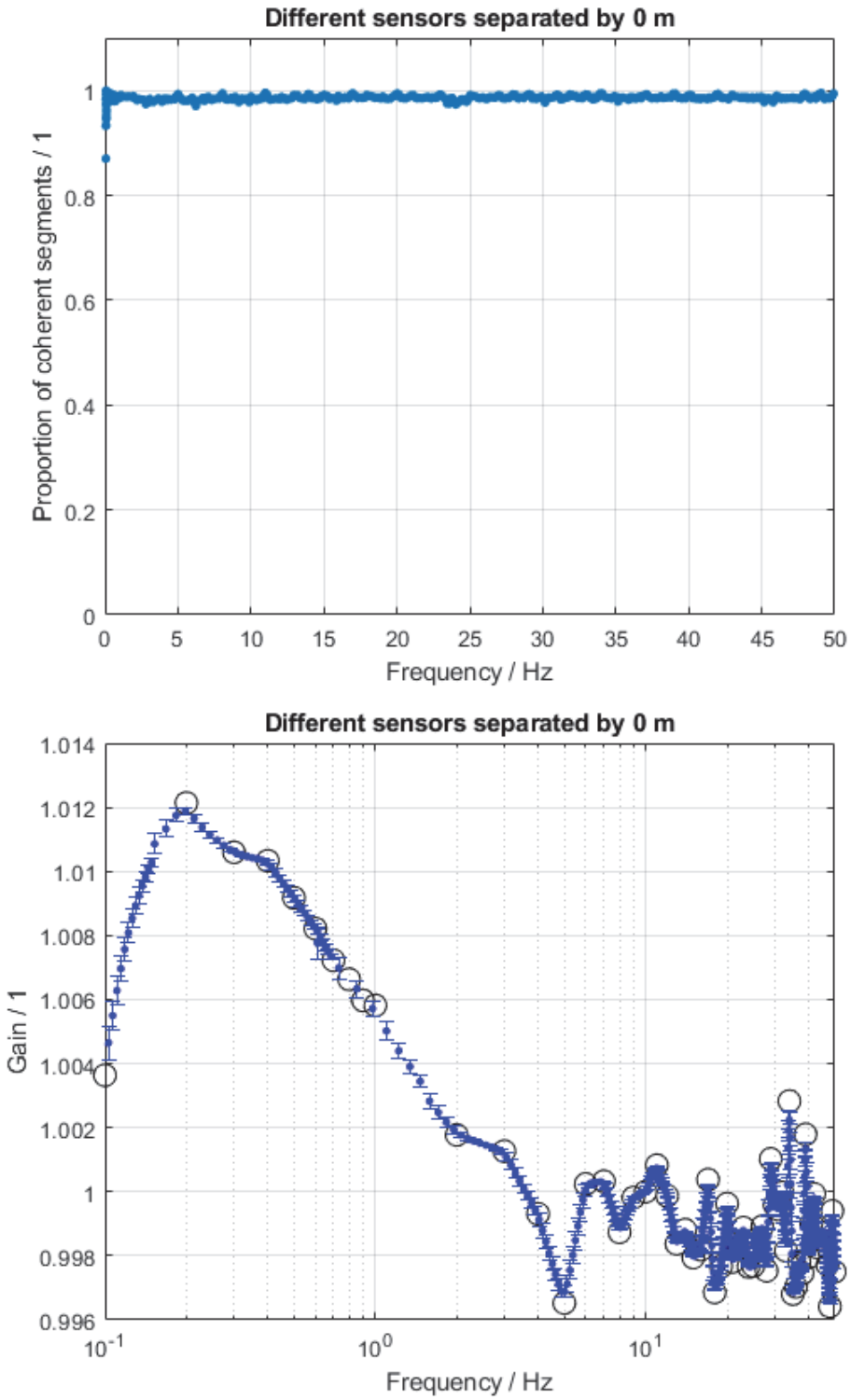

Figure 8 Results obtained using CTBTO data and Case B (different sensors that are co-located). The top graph shows the proportion of time segments for which the magnitude-squared coherence function exceeds the threshold of 0.98. The bottom graph compares the known magnitude of the gain (black circles) with the estimates (shown as blue dots) and their uncertainties (uncertainty bars with semi-widths equal to twice the standard uncertainty).

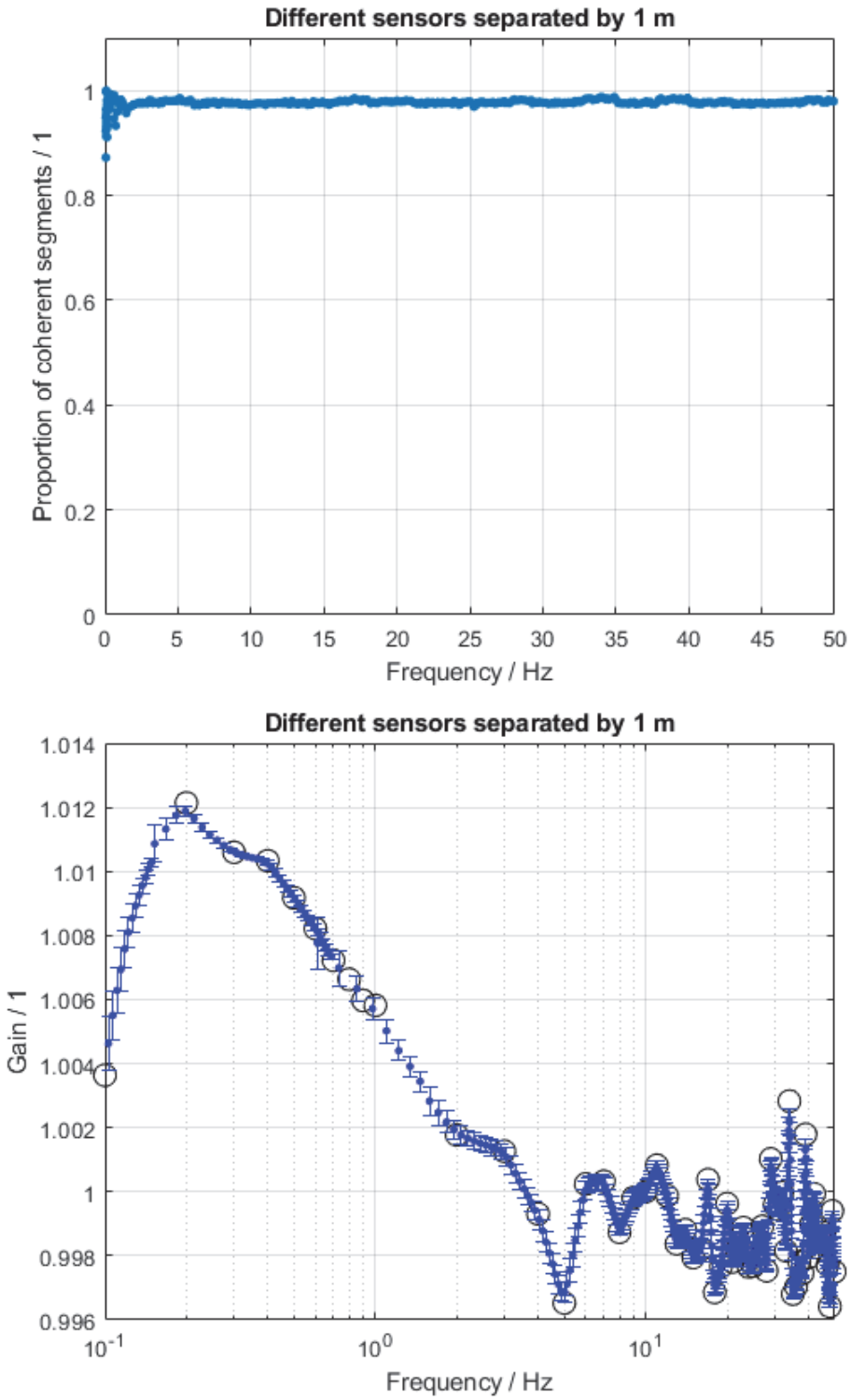

Figure 9 As Figure 8 but for Case C and the sensors are separated by 1 m.

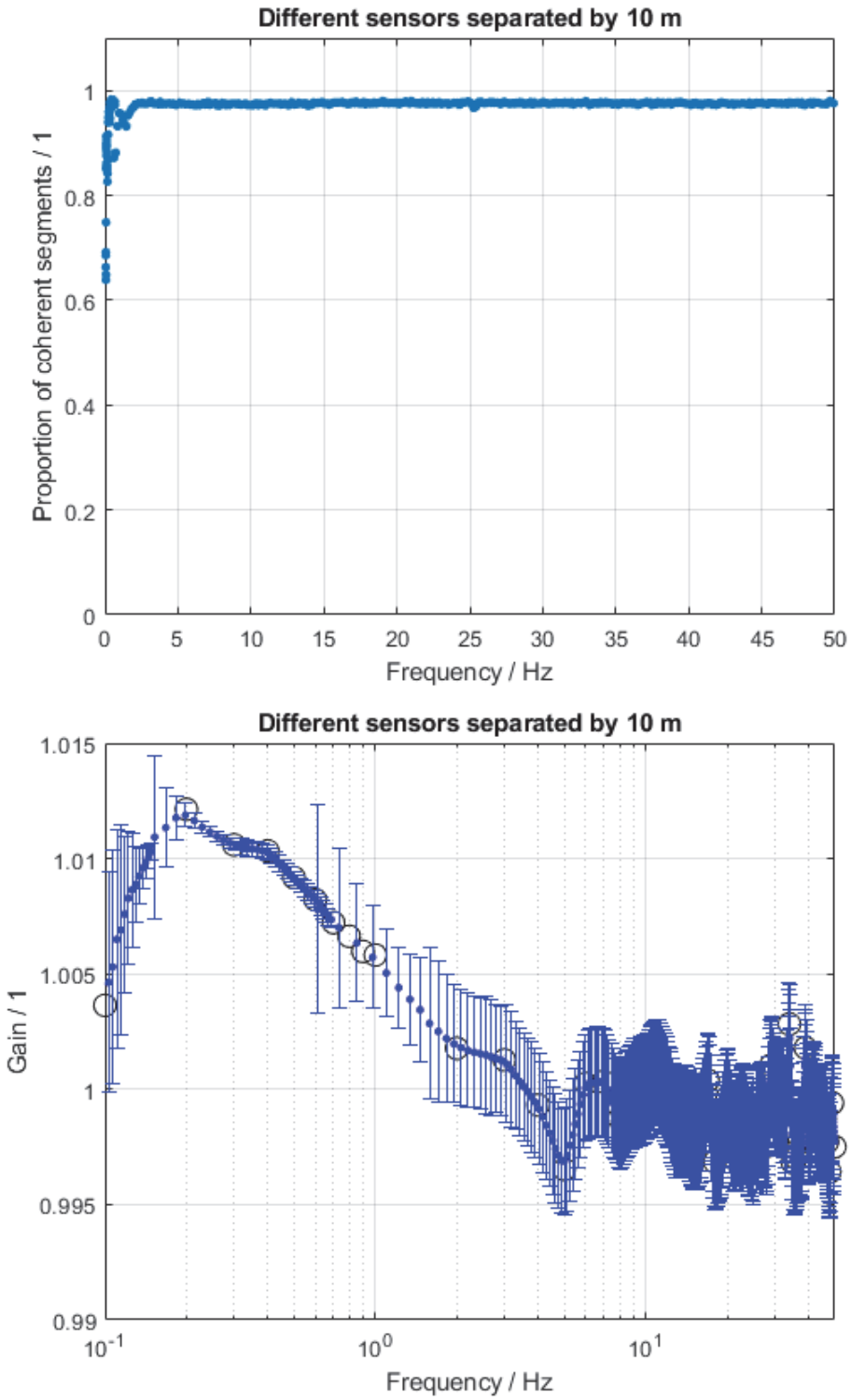

Figure 10 As Figure 8 but for Case C and the sensors are separated by 10 m.

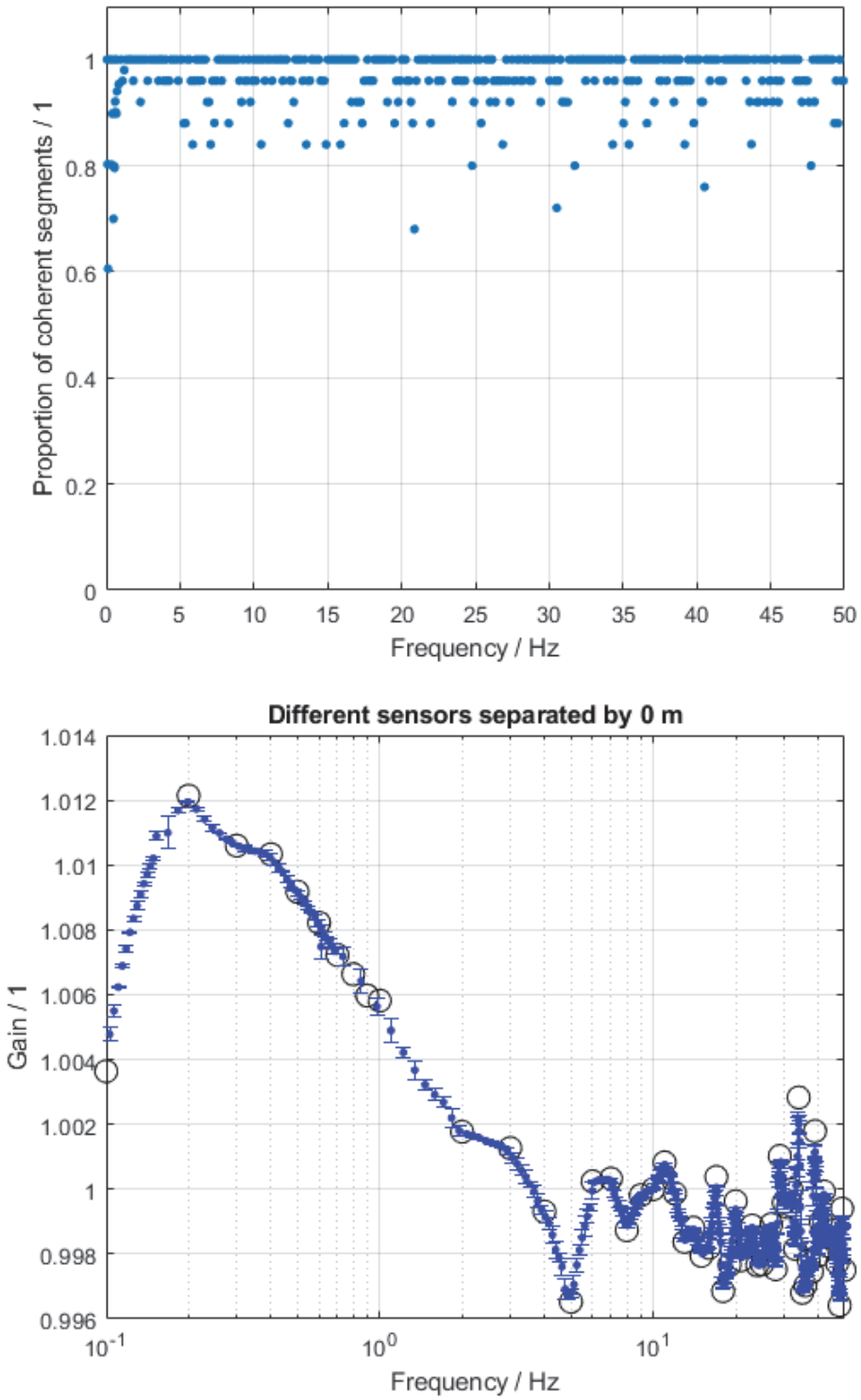

Figure 11 As Figure 8 but for using simulated data based on a simple model of how sound propagates in water and the settings $n_s = 100, S = 10\ km, R = 0\ m, H = 2\ km, m_t = 100, T = 500\ s, f_s = 250\ Hz, \Delta_s = 0\ m$.

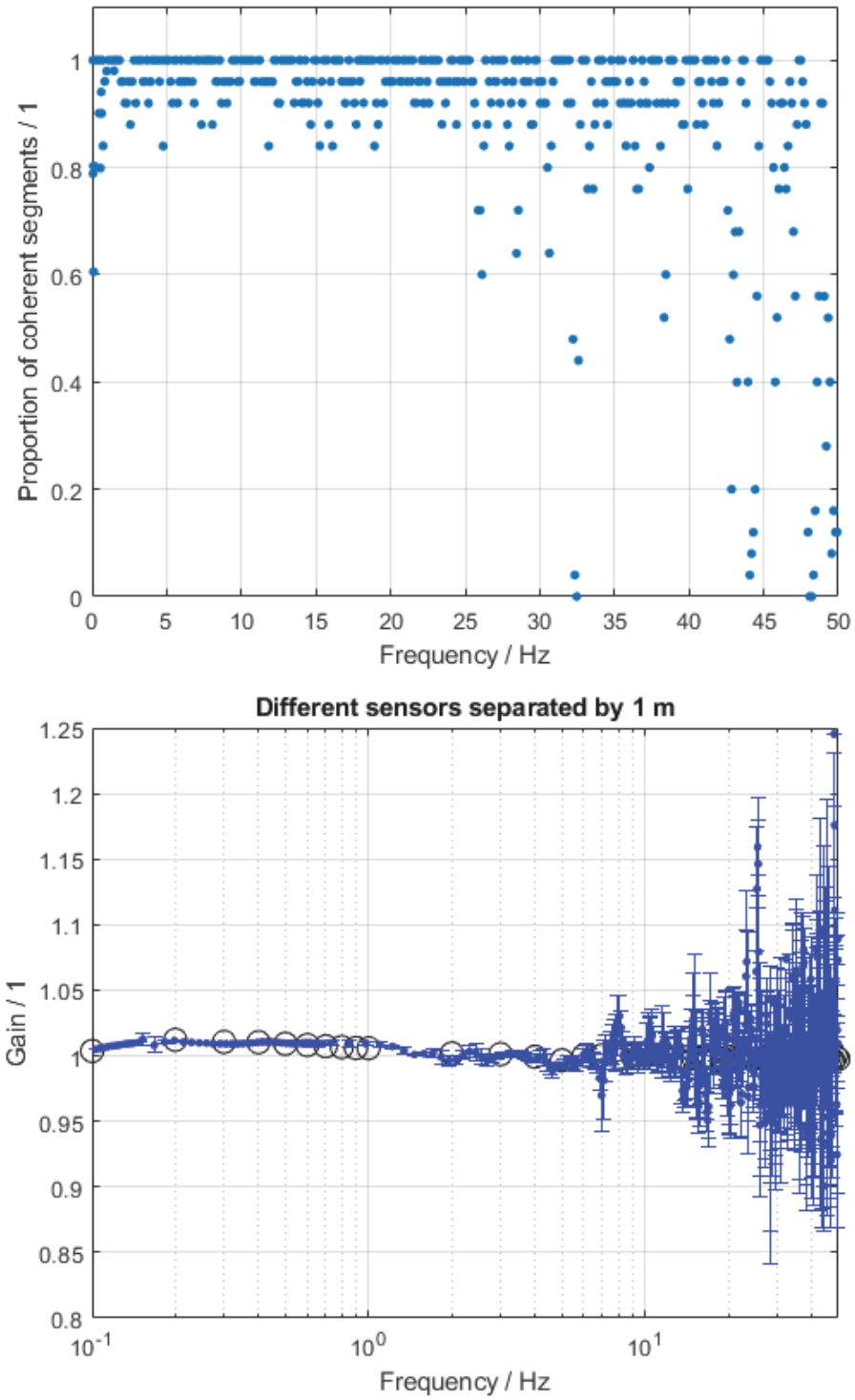

Figure 12 As Figure 11 with the same settings except $R = 1\ m$.

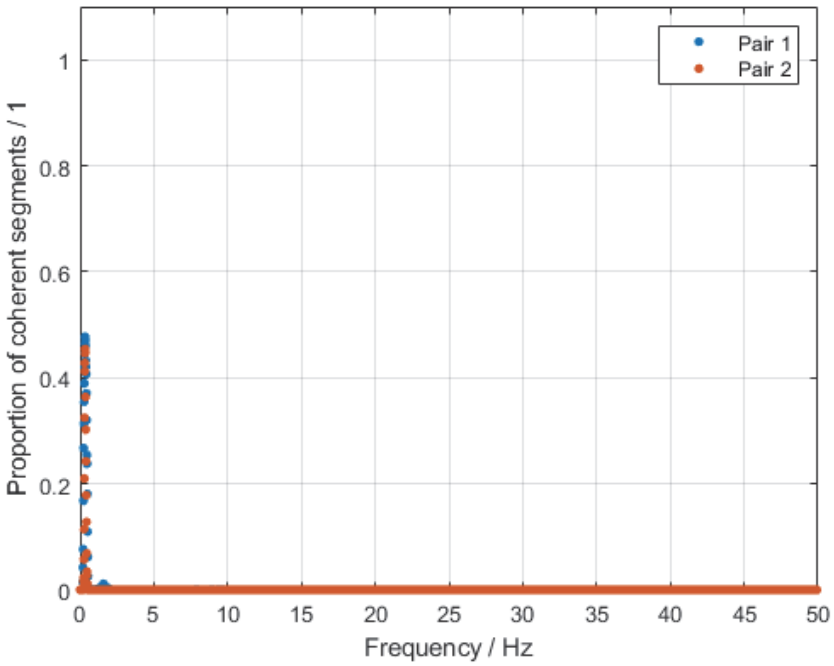

Figure 13 Using the data recorded by the hydrophones at NPL's Wraysbury reservoir, the proportion of time segments for which the magnitude-squared coherence function exceeds the threshold of 0.98 for pair 1 (channels 1 and 2) and pair 2 (channel 1 and 3).

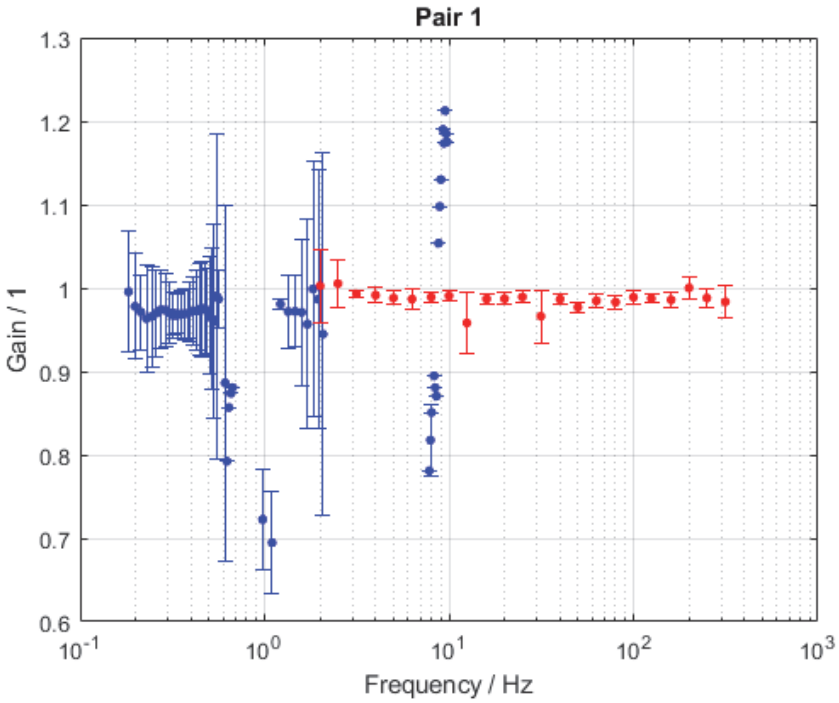

Figure 14 For pair 1 of hydrophones deployed at NPL's Wraysbury reservoir (channels 1 and 2), a comparison of the magnitude of the gain obtained from the calibrations of the hydrophones (shown as red dots with uncertainty bars) with the estimates (shown as blue dots with uncertainty bars). The uncertainty bars have semi-widths equal to twice the standard uncertainty.

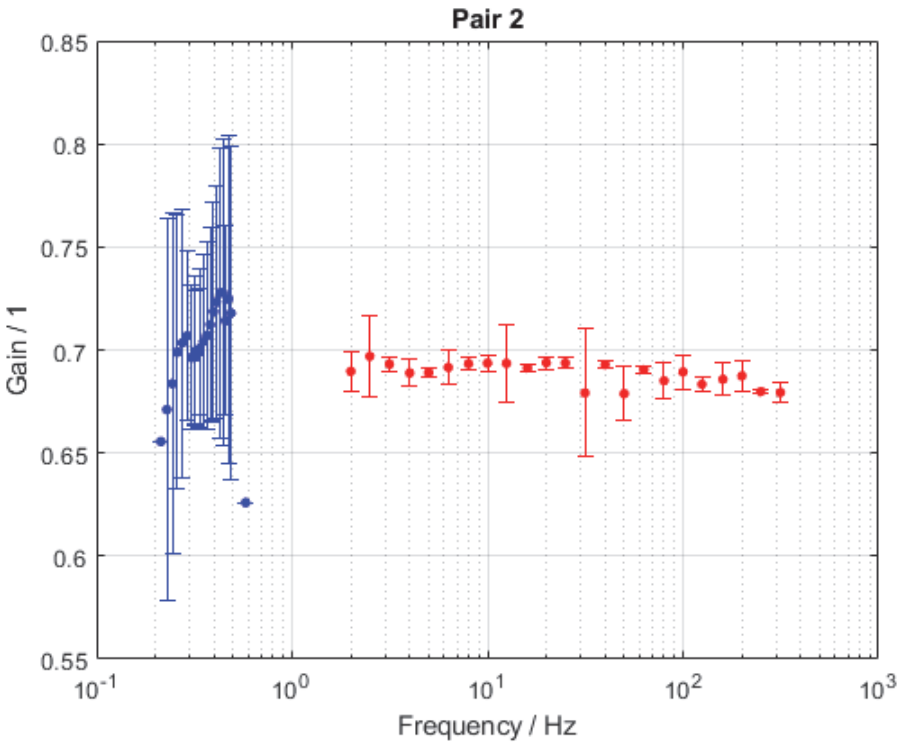

Figure 15 As Figure 14 but for pair 2 of hydrophones deployed at NPL's Wraysbury reservoir (channels 1 and 3).